*Journal of Bioenergetics and Biomembranes, Vol. 32, No. 5, 2000*

# Why Is the Mechanical Efficiency of $F_1$-ATPase So High?

**George Oster[1,3] and Hongyun Wang[2]**

The experimentally measured mechanical efficiency of the $F_1$-ATPase under viscous loading is nearly 100%, far higher than any other hydrolysis-driven molecular motor (Yasuda *et al.*, 1998). Here we give a molecular explanation for this remarkable property.

**KEY WORDS:** $F_1$-ATPase; ATP synthase; efficiency.

## INTRODUCTION

Of all the remarkable properties of the $F_1$-ATPase, perhaps the most extraordinary is its high mechanical efficiency. This was determined by measuring the average rotational velocity of an actin filament attached to the rotating $\gamma$ subunit and computing the useful mechanical work done against a viscous drag per rotation. When this divided by the free energy available from hydrolyzing three ATP's, the resulting ratio was nearly unity (Yasuda *et al.*, 1998):

$$\eta \equiv \frac{\zeta \langle \omega \rangle 2\pi}{3 \cdot \Delta G} \approx 1 \tag{1}$$

Here $\zeta$ is the Stokes rotational frictional drag coefficient of the actin filament (Happel and Brenner, 1986), $\langle \omega \rangle$ is the average rotational velocity, and $\Delta G$ is the free energy of hydrolysis. The ratio, $\eta$, might be called the "Stokes efficiency," since it is not the usual thermodynamic efficiency, which is the ratio of the output work done against a potential (i.e., a conservative force) to the input energy. The definition (1) depends on a key experimental property of the $F_1$ motor: it is *tightly coupled*. That is, the motor takes three "steps" per revolution, each step driven by the hydrolysis of one ATP (Adachi *et al.*, 2000; Yasuda *et al.*, 1998). At first glance, Eq. (1) appears to be a sensible definition of efficiency. However, because the velocity in the numerator is the *average* rotational velocity of an object whose motion is dominated by thermal fluctuations, one must exercise care in its interpretation. For example, it is not trivial to prove that $\eta \leq 1$. Thus use of this quantity deserves closer inspection, which we give in the Appendix. For now, let us accept this definition and inquire as to what properties of the $F_1$ motor are responsible for such efficient energy transduction—far higher than any other hydrolysis-driven molecular motor.

## COMPONENTS OF EFFICIENCY

The high efficiency of the $F_1$ motor rests on the following characteristics:

1. The mechanical motions are tightly coupled.
2. The chemical cycle is tightly coordinated with the mechanical rotation.
3. The motor generates a constant torque.

We will discuss the molecular basis for each of these properties and how they contribute to the mechanical efficiency.

### Tight Mechanical Coupling

The mechanical escapement that drives the rotation of the $\gamma$ subunit has been discussed elsewhere (Abrahams *et al.*, 1994; Masaike *et al.*, 2000; Oster and Wang, 2000; Wang and Oster, 1998). As shown in Fig. 1, the major conformational transition that drives the motor is a hinge-bending motion by each $\beta$ subunit that rotates helices B and C about 30° with respect to one another. This bending motion impinges on an eccentric portion of the $\gamma$ subunit

[1] Departments of Molecular and Cellular Biology and ESPM, University of California, Berkeley, California 94720-3112.
[2] School of Engineering, Department of Applied Mathematics and Statistics, University of California, Santa Cruz, California 95064.
[3] To whom correspondence should be addressed.



0145-479X/00/1000-0459$18.00/0 

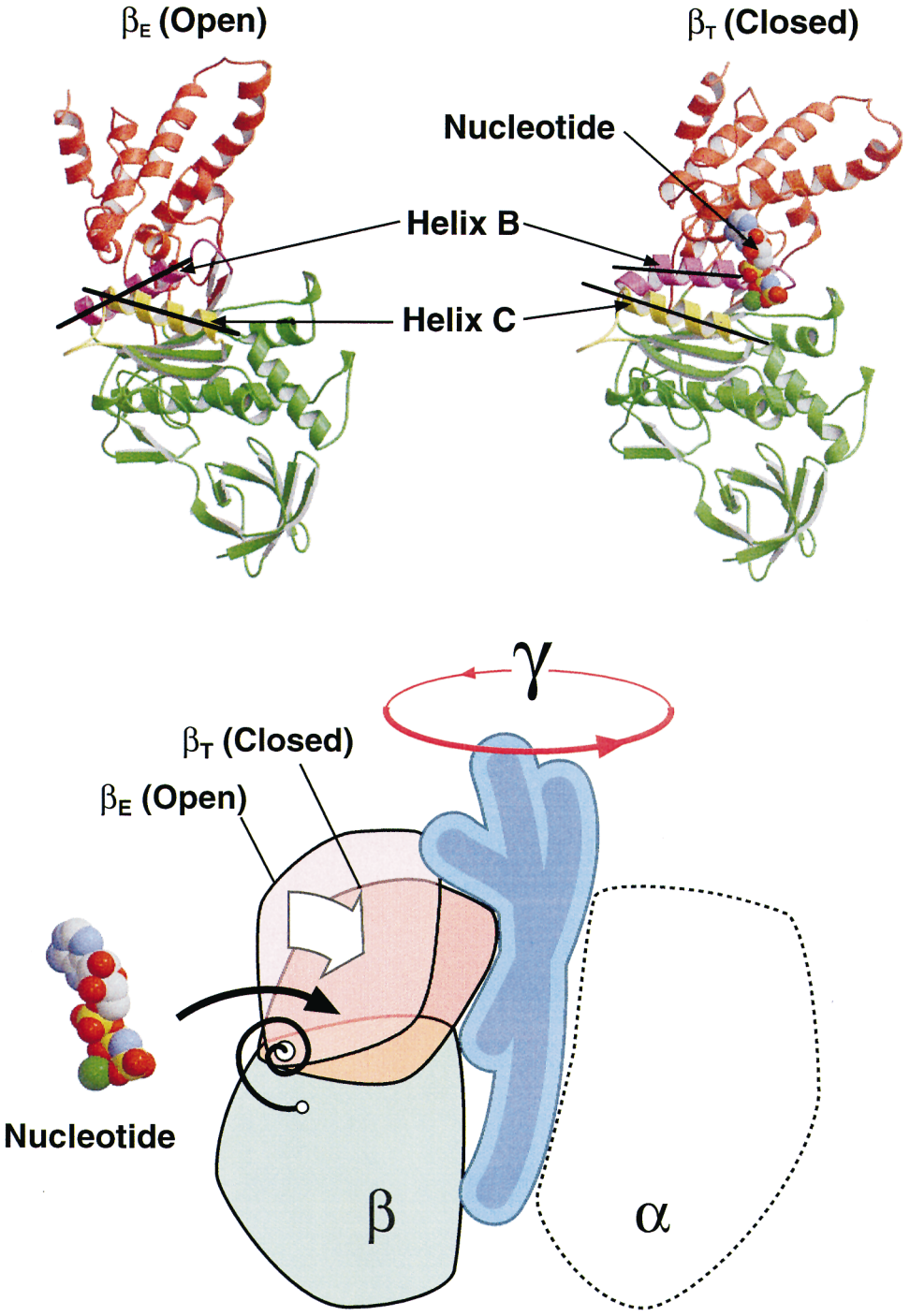


**Fig. 1.** The mechanical escapement of the $F_1$ motor. (Upper panel) During each power stroke of the $F_1$ motor the $\beta$ subunit undergoes a hinge-bending motion that closes the angle between helix B and C by about 30°, corresponding to the transition from the open state ($\beta_E$ with the catalytic site empty) to the closed state ($\beta_T$ with the catalytic site occupied by nucleotide). (Lower panel) the rotation of the upper portion of $\beta$ with respect to the lower portion entails a deformation away from the rest conformation, $\beta_E$. This stores elastic energy in the structure (note the deformation of helix B), which we denote schematically by the coil spring at the hinge point. Bending of $\beta$ pushes on $\gamma$, which, because it is bent eccentrically off axis, rotates *continuously* with the bending of $\beta$. This drives the rotation of $\gamma$ about 180° over the full bending motion of $\beta$. Thus the power strokes of the three $\beta$'s overlap so that there are no "dead spots" where the motor "hangs up".

causing it to rotate, much like turning the crankshaft of a car. Thus the "power stroke" of the $F_1$ motor is the bending of each $\beta$ subunit. Because the $\gamma$ shaft is eccentrically bent off-axis, this bending motion is converted into a rotary motion of $\gamma$. Three features of this geometric arrangement make it an efficient mechanical escapement.

1. The rotation of $\gamma$ is "lubricated." The region near the C-terminus end of the $\gamma$ shaft is hydrophobic and rotates within a hydrophobic "sleeve" formed by the $\alpha_3\beta_3$ hexamer (Abrahams *et al.*, 1994). Thus the interface between the counter-rotating subunits forms a lubricated bearing that minimizes frictional losses; that is, as $\gamma$ rotates, no strong intermolecular bonds are broken and reformed (Tawada and Sekimoto, 1991).
2. The bending of each $\beta$ subunit is tightly coupled to the rotation of the $\gamma$ shaft. That is, there is very little room for the $\gamma$ subunit to rattle around in its enclosing sleeve, so that the bending motions of each $\beta$ subunit are tightly coupled to the rotation of $\gamma$.
3. The full range of the bending motion of each $\beta$ subunit is coupled to one-half revolution of $\gamma$. Thus, the bending motions of three $\beta$'s can be coordinated to cover a full revolution with no "dead spots" where the motor could "hang up."

## Mechanochemical Coordination

Multisite hydrolysis enjoys more than a $10^5$-fold rate increase over unisite hydrolysis. Although during multisite rotation there are occasional single-step reversals, these are relatively infrequent (Noji *et al.*, 1997; Yasuda *et al.*, 1998). Therefore, the hydrolysis cycle at each catalytic site is closely coordinated with the rotational position of the $\gamma$ shaft. This means that ATP must be admitted to each catalytic site and products released in a tightly controlled rotational sequence.

Proper coordination and sequencing of rotation and catalysis is necessary for efficient energy transduction during synthesis as well as in hydrolysis mode. The mechanism of coordination is undoubtedly mechanical strain. There is strong evidence for strain coupling in other multimeric molecular motors, e.g., myosin (Walker *et al.*, 2000), kinesin (Block, 1998; Peskin and Oster, 1995; Vale and Milligan, 2000), and GroEL (Rye *et al.*, 1997; Sigler *et al.*, 1998). In $F_1$, mechanical signaling between catalytic sites can be accomplished via the intervening $\alpha$ subunits and the rotational position of $\gamma$. There is evidence for both types of signaling (Al-Shawi and Nakamoto, 1997; Ren and Allison, 2000). Mechanical signaling can control the catalytic cycle in three ways: (1) controlling the admission of nucleotide to a catalytic site (ATP gate), (2) controlling the release of product (ADP and/or $P_i$ gate), and (3) repositioning of catalytic residues. Because of Brownian motion, repositioning of catalytic residues is more difficult to achieve than substrate or product gating since the latter requires far less precision in stress propagation (although see Ren and Allison, 2000).

## Constant Torque

Experiments on the $F_1$ motor have established that the rotation of $\gamma$ proceeds stepwise, with three steps per revolution, and that each step requires the hydrolysis of one ATP (Adachi *et al.*, 2000; Yasuda *et al.*, 1998). The torque generated during multisite rotation was estimated to be about 40 pN/nm, and the Stokes efficiency in Eq. (1) was computed to be nearly 100% (see Appendix) (Yasuda *et al.*, 1998). Yet even the tight mechanochemical coupling constraints described above are not sufficient to achieve this remarkably high efficiency. One more ingredient is necessary: *the motor must generate a nearly constant torque*. In fact, we show in the Appendix that a Stokes efficiency of 100% can *only* be achieved if the motor torque is constant. Thus measurements of the $F_1$ motor torque showing that it is nearly constant complement and reinforce the efficiency calculation (Kinosita *et al.*, 2000). Therefore, we ask: what molecular mechanism can account for constant torque generation?

Thermodynamics tells us that efficiency increases if energetic transactions proceed in "small steps," the more the better. However, the $F_1$ motor takes three large steps per revolution. Moreover, if the mechanical coordination between catalytic sites is accomplished via substrate or product "gating," then the multisite free-energy diagram should resemble the unisite free-energy diagram, that shows two large drops: $\Delta G \sim 14\ k_BT$ accompanying ATP binding and $\Delta G \sim 10\ k_BT$ accompanying phosphate release (Senior, 1992; Weber and Senior, 1997). There is very little free-energy change accompanying hydrolysis or ADP release—the former is a central feature of Boyer's binding-change mechanism (Boyer, 1998, 2000). How are we to reconcile these large steps and energy drops with the measured high efficiency? It seems that the large rotational steps should be broken into many smaller steps and that both free-energy drops must be utilized to generate the power stroke. There appears to be only one solution to these requirements. To see what this must be, we must look more closely at the hydrolysis cycle. The overall reactions at a catalytic site is generally written as a cycle

of four *occupancy* states of the catalytic site (all steps are reversible and ATP denotes Mg-ATP):

$$\mathrm{F_1 + ATP} \underset{}{\overset{\text{Binding}\ \Delta G\sim 14k_BT}{\rightleftharpoons}} \mathrm{F_1\cdot ATP} \underset{\text{Synthesis}}{\overset{\text{Hydrolysis}\ \Delta G\sim 0}{\rightleftharpoons}} \mathrm{F_1\cdot ADP\cdot}\, P_i$$

$$\underset{}{\overset{\mathrm{P_i\ release}\ \Delta G\sim 10k_BT}{\rightleftharpoons}} \mathrm{F_1\cdot ADP + P_i} \underset{}{\overset{\text{ADP release}\ \Delta G\sim 0}{\rightleftharpoons}} \mathrm{F_1 + ADP + P_i} \quad (2)$$

Each hydrolysis cycle corresponds to a free-energy change of 20 to 24 $k_BT$ and a rotation by $2\pi/3$, not a small step. However, while each hydrolysis involves a large rotational step of $\gamma$, this can be accomplished by a sequence of much smaller torque-generating steps at the catalytic site as follows. Since both the ATP binding and $\mathrm{P_i}$ release steps must be coupled to rotation of $\gamma$, each chemical occupancy state in Eq. (2) represents the lowest *energy* state. Note that the ATP-binding step refers to the transformation of the catalytic site from the empty state all the way to the state where ATP is tightly bound. Thus *the binding step includes the process wherein ATP diffuses into the catalytic site and the subsequent annealing into the tightly bound state*. The phosphate release step consists of the phosphate leaving the catalytic site *and* the subsequent relaxation of the system to the lowest energy state for ADP occupancy. This means that *the rotation of the $\gamma$ subunit by $2\pi/3$ cannot be accurately represented by a single thermally activated kinetic step since the free-energy change involved is much larger than thermal energy ($k_BT$) and the rotational angle of $\gamma$ is continuous.*

Transition-state analogs show that the tight binding state involves 15–20 hydrogen bonds between Mg-ATP and the catalytic site (Abrahams *et al.*, 1994; Bianchet *et al.*, 1998; Leslie and Walker, 2000; Lobau *et al.*, 1998; Nadanaciva *et al.*, 1999). We conclude that ATP binding involves the *progressive* formation of hydrogen bonds as the nucleotide thermally settles into the catalytic site. Therefore, we can redefine the "chemical state" of the catalytic site to include, in addition to the occupancy, *the number of hydrogen bonds formed between the catalytic site and the nucleotide*. Then the generalization of Eq. (2) in the hydrolysis direction should be written as:

$$\mathrm{F_1 + ATP} \underset{}{\overset{\text{ATP docking}}{\rightleftharpoons}} \underbrace{\mathrm{F_1\cdot ATP}(\theta)}_{\text{ATP weakly bound}} \overset{\rightarrow}{\leftarrow} \cdots \underset{}{\overset{\text{Binding transition}}{\rightleftharpoons}} \cdots$$

$$\overset{\rightarrow}{\leftarrow} \underbrace{\mathrm{F_1\bullet ATP}(\theta)}_{\text{ATP tightly bound}} \underset{}{\overset{\text{Hydrolysis}}{\rightleftharpoons}} \mathrm{F_1\cdot ADP\cdot P_i} \underset{}{\overset{\mathrm{P_i\ release}}{\rightleftharpoons}}$$

$$\mathrm{F_1\cdot ADP + P_i} \underset{}{\overset{\text{ADP release}}{\rightleftharpoons}} \mathrm{F_1 + ADP + P_i} \quad (3)$$

Here the large dot distinguishes the tight binding state at the end of the binding transition from the weak binding state when ATP first enters the catalytic site. Equation (3) decomposes the binding step in Eq. (2) into ATP docking followed by a sequence of substeps corresponding to the zipping of bonds between ATP and the catalytic site. Thus the free-energy change during the binding-transition process should be viewed as a sequence of small free-energy drops rather than a single large free-energy drop. This is essentially a generalization of Boyer's binding-change mechanism to take into account the continuous rotation of $\gamma$ accompanying the binding transition following successful docking (Boyer, 1993). Figure 2 shows how the

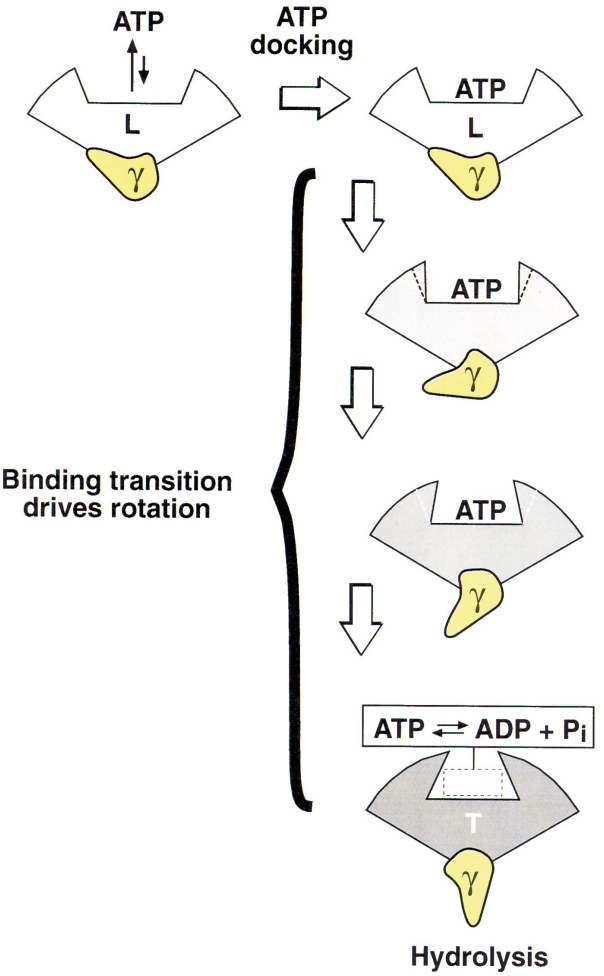


**Fig. 2.** Extending the binding-change mechanism in the hydrolysis direction to include ATP docking and the binding transition. In the binding-change diagram, ATP binding (L → T) is one kinetic step corresponding to a rotation of the $\gamma$ shaft by 120°. In the binding-zipper model, rotation of the $\gamma$ shaft is a *continuous* variable, $\theta$ (Oster and Wang, 2000; Wang and Oster, 1998). This takes into account the sequence of ~15 kinetic steps of the binding transition as the nucleotide successively anneals its hydrogen bonds to the catalytic site.

ATP-binding step of the binding-change mechanism is extended to include ATP docking and the subsequent binding transition.

Since the incoming nucleotide is hydrated, the binding transition requires that both the nucleotide and the open catalytic site break their hydrogen bonds with water molecules to form hydrogen bonds with each other. The details of the binding process are complex (Fersht, 1999). Formation of the hydrogen bonds between the nucleotide and the catalytic site entails both entropic and enthalpic changes. As each bond between the nucleotide and the catalytic site forms, the enthalpy decreases somewhat if the hydrogen bonds between the nucleotide and the catalytic site are stronger than with water. As hydrogen bonds form between the nucleotide and the catalytic site, the nucleotide-catalytic site complex loses entropic freedom. At the same time, the water molecules released from the hydration shell of the nucleotide and the catalytic site gain entropic freedom. The entropy change of the binding transition is $\Delta S = \Delta S(\text{water}) + \Delta S(\text{nucleotide–catalytic site})$. Note that after ATP successfully docks onto the catalytic site, the binding transition no longer depends on the external ATP concentration. Overall, the gain in entropy due to the liberation of hydration waters is usually more than offset by the loss of entropy by the nucleotide–catalytic site complex (Fersht, 1999). Figure 3 illustrates the docking and binding-transition processes.

The sequential zipping of hydrogen bonds during the binding transition generates a sequence of torque increments tending to close the bending angle of the $\beta$ subunit. Because of the tight mechanical coupling discussed above, this translates into a progressive torque on the $\gamma$ subunit which also consists of a sequence of steps. However, thermal fluctuations coupled with the elasticity of the $\gamma$ subunit acts to smooth the output motion, although the power stroke is generated by a sequence of small torque steps.

Since both free-energy drops must be utilized to match the measured efficiency, the torque generated during the binding transition must be used to drive the rotation of $\gamma$ in two steps. Part of the torque is delivered to $\gamma$ directly during the binding transition (the "primary power stroke"). The rest is stored as elastic strain energy as $\beta$ bends away from its rest configuration, $\beta_{\mathrm{E}}$. Following phosphate release, this stored elastic energy drives the recoil of $\beta$ to its rest state, $\beta_{\mathrm{E}}$, generating a secondary (recoil) power stroke. Because of the tight mechanochemical coupling, this happens during the binding transition of the next catalytic site in the binding change sequence so that the secondary power stroke of each catalytic site assists the primary power stroke of the next catalytic site. Thus each hydrolysis cycle drives two power strokes, further smoothing out the overall torque applied to the $\gamma$ shaft. Under unisite conditions, the free-energy change of the ATP binding step *measured externally* shows only the energy delivered to $\gamma$ during the primary power stroke. Later, following the phosphate-release step, the free-energy change measured externally reveals the energy stored as elastic strain during the binding transition and released in the recoil power stroke.

## Hydrolysis Permits Product Release

Since there is almost no free-energy change accompanying the hydrolysis step in Eq. (3), what role does hydrolysis play in torque generation? As with the binding step, the answer to this question lies in the details of the catalytic process. At the transition state, Mg-ATP is held in place by about 15–20 hydrogen bonds, amounting to a free-energy well $\sim$24 $k_BT$ deep (Bianchet *et al.*, 1998; Ko *et al.*, 1999; Nadanaciva *et al.*, 1999; Weber *et al.*, 1998). However, the equilibrium constant for the hydrolysis step is nearly unity (Boyer, 1993) and the enthalpy change for the hydrolysis cycle is only 8–9 $k_BT$ most of which can be accounted for by the electrostatic repulsion between the products (Golding *et al.*, 1996; Mathews *et al.*, 2000). The remaining 15–16 $k_BT$ of hydrolysis free energy are entropic factors that take place after product release *outside* the catalytic site and so cannot participate directly in force generation or weakening the product binding.

Previously, we have proposed that the mechanism for product release uses the enthalpy of electrostatic repulsion between the charged hydrolysis products to reduce substrate binding so that products can dislodged from the catalytic site by thermal fluctuations (Oster and Wang, 2000). This process is energetically feasible since electrostatic repulsion between ADP and phosphate is sufficient to disorient and weaken the hydrogen bonds, reducing the 24 $k_BT$ of binding energy to less than 16 $k_BT$, divided between the two products. The recoil elastic energy stored in $\beta$ during ATP binding also assists in unzipping the hydrogen bonds holding the phosphate in the catalytic site. Thus the free-energy barrier to dissociation is lowered so that thermal fluctuations quickly release the phosphate from the catalytic site. Release is rectified by the entropic increase as products diffuse away into solution. As measured externally, it appears as if the recoil power stroke is triggered by phosphate release; however, it is more correct mechanistically to say that the recoil power stroke triggers phosphate release.

It is worth noting that during synthesis the nucleotide switches between ATP and $\mathrm{ADP} + \mathrm{P_i}$ some fifty times

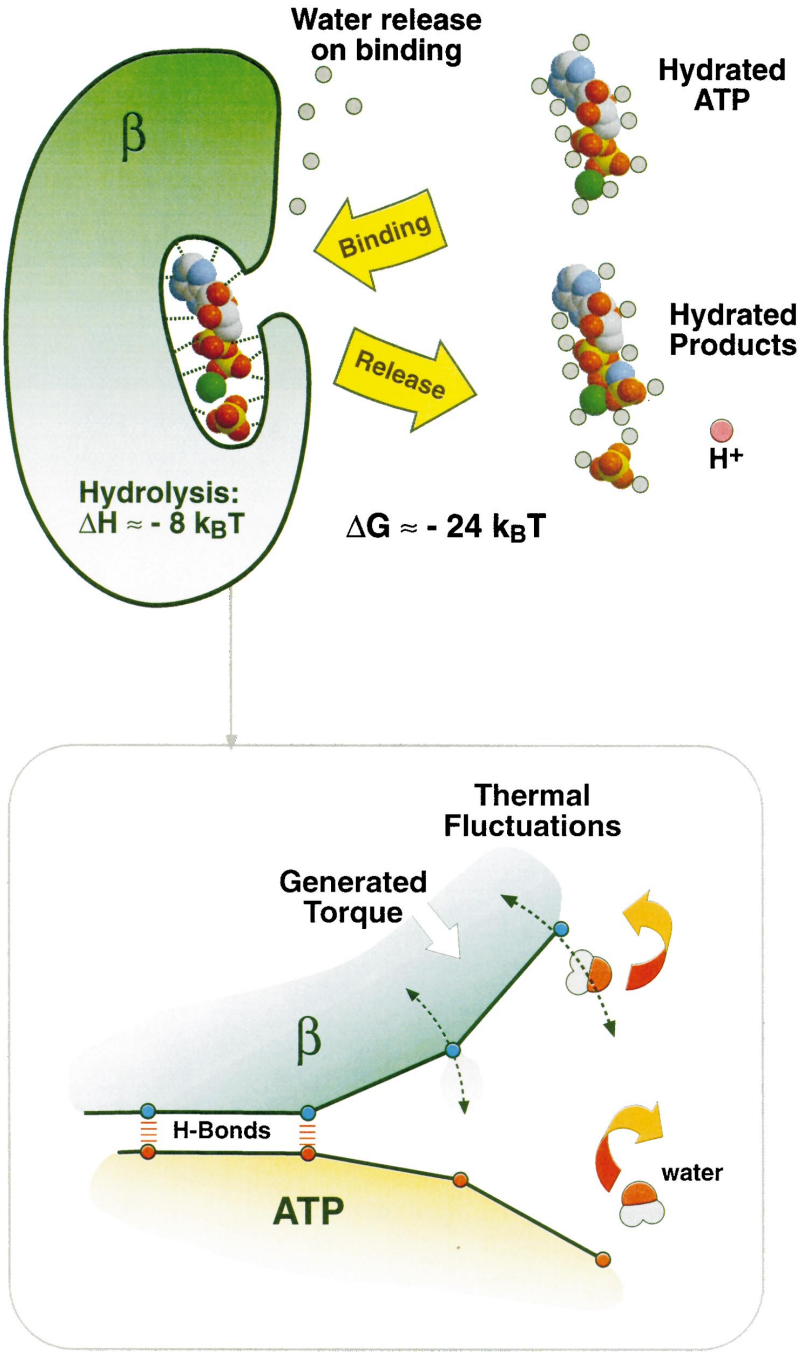


**Fig. 3.** Schematic of the catalytic site showing how the sequential annealing of hydrogen bonds is transduced into a mechanical force. (Upper panel) Measured external to the enzyme, there is a free-energy drop of about $\Delta G \approx 14\ k_B T$ accompanying ATP binding, and about 10 $k_B T$ following phosphate release. Of this $\Delta H \approx 8\ k_B T$, can be mostly attributed to the electrostatic repulsion between ADP and $P_i$ following hydrolysis. The remaining contributions to the free energy are the resonance stabilization of the phosphate, the differential hydration of ATP vs. products (ADP and $P_i$), the release of the hydrolysis proton, and the entropic increase in translational and rotational freedom accompanying release from the catalytic site. Since these events take place outside the catalytic site, they cannot contribute directly to the power stroke. (Lower panel) Thermal fluctuations sequentially carry each hydrogen bond forming residue on the catalytic site to within range of the corresponding hydrogen bond forming site on ATP. As each bond forms, it releases two hydration water molecules: one from ATP and the other from the catalytic site. This binding process entails an enthalpy drop and/or an entropy increase (Dunitz, 1994, 1995; Fersht, 1999; Qian and Hopfield, 1996). Both the enthalpic part and the entropic part of the free-energy change in the binding transition contribute to the force generation, but the entropic part of the free-energy change in the binding transition is independent of ATP concentration.

before ATP dissociates (Boyer, 1993). This means that the enthalpy arising from the electrostatic repulsion between hydrolysis products is nearly counterbalanced by the energy of the strained hydrogen bonds, so that thermal fluctuations carry the system between reactants and products over a small free-energy barrier. The details of the hydrolysis process are discussed in more detail elsewhere (Oster and Wang, 2000).

## SUMMARY AND DISCUSSION

The experimentally measured efficiency of the $F_1$ motor is nearly 100% (Kinosita *et al.*, 1999, Yasuda *et al.*, 1998). However, this estimate is based on measuring the *average* motion of a molecular motor over a long time interval working against a viscous load. Since the movements of proteins is dominated by Brownian motion, this measure of efficiency is not the same as the usual thermodynamic efficiency. An analysis of viscously loaded protein motors shows that such high efficiencies can only be achieved if the motor has certain properties:

1. A tight mechanical escapement that couples the bending of each $\beta$ subunit to the rotation of the $\gamma$ shaft.
2. A close mechanochemical coordination between the rotation of $\gamma$ and the hydrolysis cycle so that nucleotide entry and product release occur at the correct angular displacement of $\gamma$.
3. A power stroke that generates a nearly constant torque.

The tight mechanical coupling is dictated by the structure of the interface between the $\beta$ subunits and the $\gamma$ shaft. In particular, each $\beta$ subunit impinges directly on the eccentric $\gamma$ shaft so that the bending of each $\beta$ by $\sim 30^\circ$ drives a rotation of $\gamma$ by $\sim 180^\circ$. Moreover, the $\gamma$ shaft rotates within a hydrophobic sleeve formed by the $\alpha_3\beta_3$ hexamer, so that its motion is nearly frictionless. Tight mechanochemical coupling requires that the chemical cycle at each catalytic site be coordinated with the rotation of $\gamma$. This is accomplished by coupling the strain generated by ATP binding at each catalytic site to the adjacent catalytic sites via the intervening $\alpha$ subunits and by the strain generated by the rotation of the eccentric $\gamma$ shaft. These structural features are necessary, but not sufficient, to account for the high efficiency. The sufficient condition is supplied by the nature of the energy transduction process at the catalytic sites, a process we previously have nicknamed the "binding zipper" (Oster and Wang, 2000).

The high efficiency requires that the torque generated by the $F_1$ motor be nearly constant and that both the free-energy drop accompanying ATP binding and phosphate release be used to generate this torque. The simplest—and perhaps only—way to fulfill these requirements is by generalizing the binding-change mechanism to include a multistate transition from weak to strong binding as the hydrogen bonds sequentially anneal Mg-ATP to the catalytic site. This drives the primary power stroke. The second free-energy drop following phosphate release drives the recoil of the bent $\beta$ subunit to its unstrained state, releasing the elastic energy stored during the primary power stroke. A detailed calculation shows that the binding-zipper mechanism fits the observed mechanical, kinetic, and thermodynamic measurements on the $F_1$ motor (Oster and Wang, 2000; Wang and Oster, 1998). Putting the torque-generating step anywhere else in the hydrolysis cycle cannot accommodate the experimental observations. Moreover, the binding-zipper mechanism provides the most efficient (*i.e*, lossless) mechanism for utilizing the rotary torque applied to the $\gamma$ shaft by the $F_0$ motor to release the newly synthesized ATP from the catalytic site (Elston *et al.*, 1998; Oster and Wang, 2000; Wang and Oster, 1998). Placing the power stroke directly on the ATP binding step is in accord with other observations as well: (1) the power stroke of GroEL accompanies ATP binding (Bukau and Horwich, 1998); and (2) Mg-ATP, but not other metal ions, including Ca-ATP, supports rotary torque (Gromet-Elhanan and Weiss, 1989, Papageorgiou *et al.*, 1998). In the absence of Mg, the ATP binding affinity of the catalytic site is low and the ATP binding transition cannot proceed (Weber and Senior, 1997).

The design features of the $F_1$ motor shed light on why other hydrolysis motors are much less efficient energy transducers. First, the mechanochemical cycles of the "walking motors", myosin and kinesin, both involve (1) large diffusion steps during which the active driving force is zero and (2) dissociation of heads from the track, which diverts part of the hydrolysis free energy to the entropic freedom of the free head. When the rear head switches from strong to weak binding, it is pulled forward to a position ahead of the bound head. The force propelling this motion is attributed to strain energy stored in the bound head and neck region. Part of the free energy goes to the entropic freedom gained by the free head. This part of free energy does not contribute to the force generation, and thus is wasted. To proceed, the free head must diffuse to the next binding site on the track (actin or microtubule) which, depending on the load, can be a substantial distance away from the equilibrium position of the free head. Note that this diffusion step is a ratchet step that has no active driving force and that is rectified upon the binding

of the former free head to the next site. Second, the strain energy stored upon nucleotide binding in $F_1$ is directed entirely to rotation of $\gamma$. However, in myosin and kinesin part of the nucleotide binding strain is transferred to the track binding site where it is used to weaken the binding and dissociate the head from the track. For a "walking motor" to proceed at a fast speed, the energy used to dissociate the head from the track must be significantly larger than the binding energy of the head. Upon the rebinding of the head onto the track, part of the binding energy can be used to generate force, which is much less than the energy spent to dissociate the head from the track.

Finally, we see that the answer to the question posed by the title of this paper requires adding to the constraints imposed by biochemical and structural studies, the mechanical measurements on the $F_1$ motor, especially the constant motor torque imposed by high Stokes efficiency.

## APPENDIX: WHAT DOES VISCOUS LOADING MEASURE?

### The Stokes Efficiency

The *average* driving torque generated by the $F_1$ motor, $\langle\tau\rangle$ is determined by measuring the *average* rotational velocity $\langle\omega\rangle$ of an actin filament attached to the rotating $\gamma$ subunit and multiplying it by the Stokes drag coefficient, $\zeta$, of the large actin filament: $\langle\tau\rangle = \zeta \cdot \langle\omega\rangle \cdot \zeta$ can be computed from fluid mechanics (Happel and Brenner, 1986). Yasuda *et al.* used the formula

$$\zeta = \frac{4\pi\eta L^3}{\ln(L/2r) - 0.447}$$

where $\eta$ is the viscosity of the fluid medium and $L$ and $r$ are the length and radius, respectively, of the actin filament. Here $\langle\cdot\rangle$ refers to either an average of one motor over a long time (*time average*) or an average over a large collection of motors (*ensemble average*). The useful mechanical work done against a viscous drag by the motor per revolution is the product of the average drag torque and the displacement ($2\pi$): $\zeta\ 2\pi\langle\tau\rangle$. When this is divided by the free energy available from hydrolyzing three ATP's per revolution, a mechanical efficiency can be defined by:

$$\eta_{\text{Stokes}} = \frac{\overbrace{\zeta\langle\omega\rangle 2\pi}^{\substack{\text{Useful}\\ \text{mechanical work}}}}{\underbrace{3\cdot(-\Delta G_{\text{ATP}})}_{\substack{\text{free-energy}\\ \text{consumption}}}} \approx 100\% \qquad \text{(A1)}$$

We shall call this ratio the "Stokes efficiency," since it measures how effective the motor can utilize the free energy of hydrolysis to drive its cargo (the actin filament in the experiment of $F_1$-ATPase) through the surrounding viscous fluid. The Stokes efficiency is not the usual thermodynamic efficiency, which is the ratio of the work done against a conservative force to the input energy (see below). $\eta_{\text{Stokes}}$ appears to be a sensible definition of efficiency; however, because both the motor motion and the chemical reaction associated with it are dominated by thermal fluctuations, interpretation of Eq. (A1) is not as straightforward as it seems.

Consider the *total* work done by the motor on the surrounding fluid per rotation divided by the free-energy consumption per rotation. The total work done on the surrounding fluid includes *both* the work done via the motor motion (the rotation of the actin filament and the $\gamma$ subunit in the $F_1$-ATPase experiment) *and* the work done via the interaction between the catalytic sites and the environment. For example, when thermal fluctuations are captured to initiate product release, heat is absorbed by the catalytic sites from the environment. *Both* of these two terms can be negative! The total work done on the surrounding fluid is the heat released in the overall hydrolysis cycle, which is the enthalpy component of the free-energy change. This can be *larger* than $\Delta G$ and also can be negative. For example, when charged particles are driven by a voltage difference against a concentration gradient, the amount of heat released is *greater than* the free-energy change involved in moving the particle up the gradient. Conversely, when charged particles are driven by a concentration gradient against a voltage difference, heat is absorbed in the reaction and the work done on the surroundings is negative.

One might be tempted to measure the efficiency of a motor by computing the work done on the surrounding fluid via the motor motion per cycle (which is dissipated as heat) divided by the free-energy consumption per cycle (Sekimoto, 1997).

$$\eta_{\text{heat}} \equiv \frac{\text{work done on the fluid environment by the motor motion per reaction cycle}}{\text{free-energy consumption per reaction cycle}}$$

Unfortunately, $\eta_{\text{heat}}$ is neither bounded by 100% from above nor bounded by zero from below. $\eta_{\text{heat}}$ can approach 100%—or even exceed 100%—yet this does not necessarily imply that the motor is operating at its maximum possible performance. Therefore, it is inappropriate to use $\eta_{\text{heat}}$ to measure the efficiency of molecular motors.

If the Stokes efficiency defined in Eq. (A1) is not bounded by 100%, then the near 100% Stokes efficiency is not the maximum performance of a motor, and thus may not be so remarkable. It is not trivial to prove that $\eta_{\text{Stokes}} \leq 1$. In Oster and Wang (2000), we showed that the Stokes efficiency is bounded by one when the motor is driven by a tilted periodic potential. The mathematical formulation and proof for the general case will be given elsewhere.

## Comparison of Stokes Efficiency to Thermodynamic Efficiency

### *High Thermodymanic Efficiency Implies Tight Coupling*

Consider the situation where a motor is working against an external load that can be described by a potential function, $F_{\text{load}} = -\partial V/\partial\theta$, *i.e.*, the load force is conservative. For example, a laser trap can be accurately described by a quadratic potential, analogous to an elastic spring: $V = 1/2\kappa(x - x_0)^2$, where $x_0$ is the location of the trap center (Svoboda and Block, 1994; Yin *et al.*, 1995). When the free-energy consumption per motor step is *fixed*, the chemical reaction and the motor motion are said to be *tightly coupled*. Suppose the free-energy consumption is $-\Delta G$ for a motor step of $\Delta\theta$. The *thermodynamic efficiency* is proportional to the load force the motor is working against: $F_{\text{load}}\Delta\theta/(-\Delta G)$. For kinesin dimers, $\Delta\theta = 8$ nm and $-\Delta G =$ ATP hydrolysis free energy. The *maximum* thermodynamic efficiency is achieved when the motor is working against a conservative force slightly less than the stall force (this maximum thermodynamic efficiency is sometimes simply called the "thermodynamic efficiency").

If the chemical reaction and the motor motion are tightly coupled for the *full* range of the load force, the system comes to equilibrium at the stall load and the thermodynamic efficiency is 100%. For tightly coupled motors, slowing the motor to almost stall is guaranteed to yield a thermodynamic efficiency approaching 100%. If the chemical reaction and the motor motion are *not* tightly coupled near the stall load, the motor can execute "futile chemical cycles" that do no work. In this case, the maximum thermodynamic efficiency is attained below the stall load, and consequently is less than 100%. Tightly coupling the chemical reaction and the motor motion for the full range of the load force is the *necessary and sufficient* condition for a motor to achieve a thermodynamic efficiency near 100%. Therefore, if the maximum thermodynamic efficiency approaches 100% as the motor approaches stall conditions, this tells us that the motor is tightly coupled. It does not tell us any other aspects of the motor's force-generation mechanism.

To illustrate these points, we consider a simple example where a tightly coupled motor is driven by a tilted periodic potential. The driving potential can be written as: $\phi_{\text{drive}}(\theta) = \phi(\theta) + (\Delta G/\Delta\theta)\cdot\theta$, where $\Delta\theta$ is the motor step, $\Delta G < 0$ is the free-energy change per motor step, and $\phi(\theta)$ is a "bump" potential with period $\Delta\theta$ that measures how much the motor torque deviates from constant. The stochastic motor motion is described by the Langevin equation [or the equivalent Fokker–Planck Eq. (16) in Oster and Wang, 2000]

$$\zeta \underbrace{\frac{d\theta}{dt}}_{\substack{\text{viscous}\\ \text{drag torque}}} = \underbrace{-\phi'(\theta) - \frac{\Delta G}{\Delta\theta}}_{\substack{\text{driving}\\ \text{torque}}} + \underbrace{\tau_B(t)}_{\substack{\text{Brownian}\\ \text{torque}}} \qquad \text{(A2)}$$

Here $\zeta$ is the drag coefficient of the motor *plus* the load it is driving (the actin filament in the $F_1$-ATPase experiment). Because the free-energy change is tightly coupled to the motor motion, the maximum thermodynamic efficiency is 100% regardless of the shape of the driving potential. When the driving potential has a constant slope, the motor is driven by power strokes. When the driving potential is a staircase function, the motor is driven by Brownian ratchet steps. *However, the maximum thermodynamic efficiency cannot distinguish these two extremes or anything between them.* As long as the motor motion and the chemical reaction are tightly coupled, the maximum thermodynamic efficiency is 100%.

### *High Stokes Efficiency Implies a Constant Motor Torque*

The Stokes efficiency applies to the situations where the motor is loaded by viscous drag. It can be expressed in terms of $\phi(x)$ as follows (Oster and Wang, 2000):

$$\eta_{\text{Stokes}} = \frac{\zeta\,\langle\omega(\zeta)\rangle\,\Delta\theta}{(-\Delta G)} \qquad \text{(A3)}$$

where

$$\langle \omega(\zeta) \rangle = \frac{\frac{(-\Delta G)}{\zeta \Delta\theta} \int_0^{\Delta\theta} \exp\left(\frac{\Delta G}{k_B T} \cdot \frac{s}{\Delta\theta}\right) ds}{\int_0^{\Delta\theta} \left\{ \frac{1}{\Delta\theta} \int_0^{\Delta\theta} \exp\left(\frac{\phi(s+\theta)-\phi(\theta)}{k_B T}\right) d\theta \right\} \cdot \exp\left(\frac{\Delta G}{k_B T} \frac{s}{\Delta\theta}\right) ds} \tag{A4}$$

The motor can be slowed by increasing the viscous drag load, *i.e.*, increasing the drag coefficient $\zeta$ in Eq. (A2). This can be done either by increasing the viscosity of the surrounding fluid or by increasing the size of the load (e.g., the length of the actin filament). However, notice that *the Stokes efficiency given in Eq. (A3) is independent of* $\zeta$—it cancels out in computing equation (A3). Thus, a 100% Stokes efficiency cannot be achieved by simply slowing down the motor. Equation (A4) shows that *the Stokes efficiency is determined completely by the bump potential,* $\phi(x)$. This enables us to deduce information about the driving potential from the measured Stokes efficiency. The Stokes efficiency is always *bounded* by 100% (Oster and Wang, 2000). When the bump potential $\phi(x) = 0$, the driving potential has a constant slope (the motor torque is constant) and the Stokes efficiency is 100%. The bump potential, $\phi(\theta)$, measures how the driving torque deviates from a constant $-\Delta G/\Delta\theta$. The farther the driving force deviates from a constant, the lower the Stokes efficiency (Oster and Wang, 2000). *Therefore, a Stokes efficiency approaching 100% tell us that the motor force is nearly constant.* Yasuda, *et al.* (1998) showed that the $F_1$ motor was tightly coupled and measured a Stokes efficiency of nearly 100%. Subsequent measurements showed that the $F_1$ motor torque is nearly constant (Kinosita *et al.*, 2000). The discussion above shows that these two measurements are not independent: the first implies the second, and so the experiments reinforce one another.

### *The "Viscous Stall Force" Extrapolated from Viscous Loading Measurements May Be Smaller Than the Conservative Stall Force*

The motor velocity generally decreases as the viscous drag increases. If the motor velocity is measured for a sequence of increasing drags, a "viscous stall force" can be extrapolated as $F_{\text{viscous stall}} = \lim_{\zeta \to \infty} \zeta \langle \omega(\zeta) \rangle$ (Hunt *et al.*, 1994). The thermodynamic stall force can be measured by applying a conservative force (*e.g.*, a laser trap or an elastic barrier) to stop the motor (Visscher *et al.*, 1999). For the simple example described in Eq. (A2), the thermodynamic stall force is $F_{\text{stall}} = (-\Delta G)/\Delta\theta$. The viscous stall force is

$$F_{\text{viscous stall}} = \lim_{\zeta \to \infty} \zeta \langle \omega(\zeta) \rangle \leq \frac{(-\Delta G)}{\Delta\theta}$$

The inequality holds because the term in curly brackets in Eq. (A4) is always larger than or equal to one. The farther the driving force deviates from a constant the larger this term and consequently the smaller the viscous stall force in comparison with the thermodynamic stall force. For kinesin dimers, the extrapolated viscous stall force was indeed smaller than the conservative stall force measured using a laser trap (Hunt *et al.*, 1994; Visscher *et al.*, 1999). The difference between these two kinds of stall forces suggests that the motor force from the kinesin dimers may not be very uniform. This can be attributed to the mechanochemical cycle of kinesin. When two kinesin heads are both bound on the microtubule, the link between them is stretched (Kozielski *et al.*, 1997). When one head dissociates from the microtubule, the conformational change (power stroke) on the bound head pulls the free head forward (Rice *et al.*, 1999; Vale and Milligan, 2000). However, it is unlikely that the bound head can deliver the free head precisely to the next binding site. Therefore, between power strokes, the kinesin has to find the next binding site by diffusing forward some fraction of the step (Peskin and Oster, 1995). During this diffusion process, the active driving force is zero.

## ACKNOWLEDGMENTS

GFO was supported by NSF grant DMS-9972826. HW was supported by NSF grant DMS-0077971. The authors would like to thank Paul Boyer for his extensive feedback in relating the binding zipper to the binding-change mechanism.

## REFERENCES

Abrahams, J., Leslie, A., Lutter, R., and Walker, J. (1994). *Nature (London)* **370**, 621–628.
Adachi, K., Yasuda, R., Noji, H., Itoh, H., Harada, Y., Yoshida, M., and Kinosita, K., Jr. (2000). *Proc. Natl. Acad. Sci. USA.*
Al-Shawi, M., and Nakamoto, R. (1997). *Biochemistry*, **36**, 12954–12960.
Bianchet, M., Hullihen, J., Pedersen, P., and Amzel, L. (1998). *Proc. Natl. Acad. Sci. USA* **95**, 11065–11070.
Block, S. (1998). *J. Cell Biol.* **140**, 1281–1284.
Boyer, P. (1993). *Biochim. Biophys. Acta* **1140**, 215–250.
Boyer, P. (1998). *Biochim. Biophys. Acta* **1365**, 3–9.
Boyer, P. (2000). *Biochim. Biophys. Acta* **1458**, 252–262.
Bukau, B., and Horwich, A. L. (1998). *Cell* **92**, 351–366.
Dunitz, J. D. (1994). *Science* **264**, 670.

Dunitz, J. D. (1995). *Chem. Biol.* **2**, 709–712.
Elston, T., Wang, H., and Oster, G. (1998). *Nature (London)* **391**, 510–514.
Fersht, A. (1999) *Structure and Mechanism in Protein Science: A Guide to Enzyme Catalysis and Protein Folding*, W. H. Freeman, San Francisco, California.
Golding, E., Teague, W., and Dobson, G. (1996). *J. Exp. Biol.* **199**, 509–512.
Gromet-Elhanan, Z., and Weiss, S. (1989). *Biochemistry* **28**, 3645–3650.
Happel, J., and Brenner, H. (1986) *Low Reynolds Number Hydrodynamics: With Special Applications to Particulate Media*, Vol. 1, Nijhoff, The Hague.
Hunt, A. J., Gittes, F., and Howard, J. (1994). *Biophys. J.* **67**, 766–781.
Kinosita, K., Yasuda, R., and Noji, H. (1999). In *Essays in Biochemistry* (S. Higgins, G. B., ed.), Vol. 35, Portland Press, London.
Kinosita, K., R. Yasuda, H. Noji, and K. Adachi (2000). *Phil. Trans. Biol. Sci.* **355**, 473–490.
Ko, Y. H., Hong, S. J., and Pedersen, P. L. (1999). *J. Biol. Chem.* **274**, 28853–28856.
Kozielski, F., Sack, S., Marx, A., Thormahlen, M., Schonbrunn, E., Biou, V., Thompson, A., Mandelkow, E.-M., and Mandelkow, E. (1997). *Cell* **91**, 985–994.
Leslie, A., and Walker, J. (2000). *Phil. Trans. Biol. Sci.* **355**, 465–472.
Lobau, S., Weber, J., and Senior, A. E. (1998). *Biochemistry* **37**, 10846–10853.
Masaike, T., Mitome, N., Noji, H., Muneyuki, E., Yasuda, R., Kinosita, K., and Yoshida, M. (2000). *J. Exp. Biol.* **203**, 1–8.
Mathews, C. K., Van Holde, K. E., and Ahern, K. G. (2000). *Biochemistry*, Benjamin Cummings, San Francisco, California.
Nadanaciva, S., Weber, J., and Senior, A. E. (1999). *J. Biol. Chem.* **274**, 7052–7058.
Noji, H., Yasuda, R., Yoshida, M., and Kinosita, K. (1997). *Nature (London)* **386**, 299–302.
Oster, G., and Wang, H. (2000). *Biochim. Biophys. Acta (Bioenergetics)* **1458**, 482–510.
Papageorgiou, S., Melandri, A., and Solaini, G. (1998). *J. Bioenerg. Biomembr.* **30**, 533–541.
Peskin, C. S., and Oster, G. (1995). *Biophys. J.* **68**, 202s–210s.
Qian, H., and Hopfield, J. (1996). *J. Chem. Phys.* **105**, 9292–9298.
Ren, H., and Allison, W. (2000). *Biochim. Biophys. Acta* **1458**, 221–233.
Rice, S., Lin. A., Safer, D., Hart, C., Nabe, N., Carragher, B., Cain, S., Pechatnikova, E., Wilson-Kubalek, E., Whittaker, M., Pate, E., Cook, R., Taylor, E., Milligan, R., and Vale, R. (1999). *Nature (London)* **402**, 778–784.
Rye, H. S., Burston, S. G., Fenton, W. A., Beechem, J. M., Xu, Z., Sigler, P. B., and Horwich, A. L. (1997). *Nature (London)* **388**, 792–798.
Sekimoto, K. (1997). *J. Phys. Soc. Jpn.* **66**, 1234–1237.
Senior, A. (1992). *J. Bioenergetics Biomembr.* **24**, 479–483.
Sigler, P. B., Xu, Z. H., Rye, H. S., Burston, S. G., Fenton, W. A., and Horwich, A. L. (1998). *Annu. Rev. Biochem.* **67**, 581–608.
Svoboda, K., and Block, S. (1994). *Annu. Rev. Biophys. Biomol. Struct.* **23**, 247–285.
Tawada, K., and Sekimoto, K. (1991). *J. Theoret. Biol.* **150**, 193–200.
Vale, R., and Milligan, R. (2000). *Science* **288**, 88–95.
Visscher, K., Schnitzer, M., and Block, S. (1999). *Nature (London)* **400**, 184–189.
Walker, M., Burgess, S., Sellers, J., Wang, F., Hammer, J., Trinick, J., and P. Knight (2000). *Nature (London)* **405**, 804–807.
Wang, H., and Oster, G. (1998). *Nature (London)* **396**, 279–282.
Weber, J., and Senior, A. E. (1997). *Biochim. Biophys. Acta* **1319**, 19–58.
Weber, J., Hammond, S. T., WilkeMounts, S., and Senior, A. E. (1998). *Biochemistry* **37**, 608–614.
Yasuda, R., Noji, H., Kinosita, K., and Yoshida, M. (1998). *Cell* **93**, 1117–1124.
Yin, H., Wang, M. D., Svoboda, K., Landick, R., Block, S. M., and Gelles, J. (1995). *Science* **270**, 1653–1657.